J Sci Comput (2018) 77:579–596
https://doi.org/10.1007/s10915-018-0719-5

Shock Regularization with Smoothness-Increasing Accuracy-Conserving Dirac-Delta Polynomial Kernels

B. W. Wissink[1,4] · G. B. Jacobs[1] · J. K. Ryan[2] · W. S. Don[3] · E. T. A. van der Weide[4]

Received: 24 August 2017 / Revised: 9 April 2018 / Accepted: 20 April 2018 /
Published online: 30 April 2018

Abstract A smoothness-increasing accuracy conserving filtering approach to the regularization of discontinuities is presented for single domain spectral collocation approximations of hyperbolic conservation laws. The filter is based on convolution of a polynomial kernel that approximates a delta-sequence. The kernel combines a kth order smoothness with an arbitrary number of m zero moments. The zero moments ensure a mth order accurate approximation of the delta-sequence to the delta function. Through exact quadrature the projection error of the polynomial kernel on the spectral basis is ensured to be less than the moment error. A number of test cases on the advection equation, Burger's equation and Euler equations in 1D and 2D show that the filter regularizes discontinuities while preserving high-order resolution away from a discontinuity.

Keywords Shock capturing · Hyperbolic conservation laws · Regularization · Dirac-Delta · Chebyshev collocation · Filtering

1 Introduction

Shock capturing with high-order spectral methods is well known to be plagued by Gibbs phenomena in the solution. Nonlinear polynomial reconstruction schemes such as the nonlinear weighted essentially non-oscillatory (WENO) finite difference schemes on a uniformly spaced grid that have been very successful [1] do not extend well to global polynomial based Chebyshev and Legendre collocation (spectral) methods. Since spectral methods rely on high-order global basis functions, slope limiters are often applied to suppress Gibb's oscillations.

✉ G. B. Jacobs
gjacobs@mail.sdsu.edu

1 Department of Aerospace Engineering, San Diego State University, San Diego, CA, USA

2 School of Mathematics, University of East Anglia, Norwich, UK

3 School of Mathematical Sciences, Ocean University of China, Qingdao, China

4 Faculty of Engineering Technology, University of Twente, Enschede, The Netherlands

The most common approach is to use explicit Runge Kutta Discontinuous Galerkin (RKDG) methods with min-mod slope limiters introduced by Cockburn [2,3] An extensive bibliographic reference on discontinuous Galerkin limiters can be found in [4]. A cost-effective alternative to limiting is the physics based artificial viscosity (AV) approach, e.g. [5–8] where artificial higher even order differential terms are added to the equations to dissipate the high frequency waves or smoothen the small scale structures. While this approach is very stable and more accurate than lower order alternatives, there is no formal proof of higher-order resolution and accuracy. Yet another approach is to use filtering, which has successfully been employed in simulating shocked flow [5,9]. The high order filter used there is the variable order exponential filter, which does not satisfy all the criteria for the definition of filter as laid out in [10] exactly but asymptotically.

A yet to be explored technique for shock capturing is the use of SIAC-like filters. The typical application of SIAC filtering is to obtain superconvergence. This is accomplished by using information that is already contained in the numerical solution to increase the smoothness of the field and to reduce the magnitude of the errors. The solution, as a post-processing step, is convolved against a specifically designed kernel function once at the final time. The foundations for this postprocessor were established by Bramble and Schatz [11]. They showed that the accuracy of Ritz-Galerkin discretizations can be doubled by convolving the solution against a certain kernel function. Cockburn et al. [12] used the ideas of Bramble and Schatz and those of Mock and Lax [13] to demonstrate that the postprocessor is also suitable for DG schemes. They proved that, for a certain class of linear hyperbolic equations with sufficiently smooth solutions, the postprocessor enhances the accuracy from order $k+1$ to order $2k+1$ in the L_2-norm, where k is the polynomial degree of the original DG approximation. This postprocessor relies on a symmetric convolution kernel consisting of $2k+1$ B-splines of order $k+1$.

In [14], a regularization technique is developed for the Dirac-Delta source terms in hyperbolic equations that is an excellent candidate for a kernel of a SIAC-like regularization filter of shock discontinuities. The technique is based on a class of high-order compactly supported piecewise polynomials introduced in [15]. The piecewise polynomials provide a high-order approximation to the Dirac-Delta whose overall accuracy is controlled by two conditions: *the number of vanishing moments* and *smoothness*. SIAC kernels have similar smoothness and moment properties as the Dirac-Delta kernel, but are based on piecewise continuous B-splines instead of polynomials. In [16] it was shown that SIAC-like filters based on the compactly supported Dirac-Delta kernels capture particle-fluid interface discontinuities with higher-order resolution in single domain spectral solutions. The compactness of support is closely related to the moment condition. Smoothness properties yield higher-order resolution away from the discontinuity.

In the present work we have developed SIAC-like filters based on the high-order Dirac-Delta kernel for the regularization of shocks and discontinuities. The filter operation is based on convolution of the solution with the high-order Dirac-Delta kernels. The formulation of the operation is derived and written in matrix-vector multiplication form to allow for an efficient and simple implementation. The filters are tested on a spectral solver for hyperbolic conservation laws, such as the one and two dimensional scalar linear advection equation, one dimensional scalar nonlinear Burgers' equation, and both one- and two-dimensional nonlinear Euler equations. For the solution to the linear advection equation a filtered discontinuous initial condition is advected according to the theoretical estimate that depends on the support width and number of vanishing moments on the kernel. The support width depends on the grid-spacing and the number of vanishing moments. For the non-linear Burgers' and Euler equations, the filter has to be applied at every time step in order to regain smoothness and

stability. A sufficiently accurate Dirac-Delta kernel and small support-width, leads to good accuracy with minimal errors away from the discontinuity as well.

In Sect. 2 the filter-operation is derived and background information about SIAC filters, the high-order Dirac-Delta functions and the Chebyshev collocation method is provided. Section 3 presents and discusses the numerical results. Section 4 summarizes the results and gives an outlook for future work.

2 Formulation and Methodology

2.1 Chebyshev Collocation Method

Global polynomial based spectral methods, in this particular case, the Chebyshev collocation method, are commonly used in the discretization of spatial derivatives in PDE's since the order of convergence, for a sufficiently smooth function, depends only on the smoothness of the solution, also known as spectral accuracy. For example, the truncation error of the spectral approximation of a C^p function is at least $O(N^{-p})$. In the case of an analytical function, the order of convergence of the approximation is exponential [17]. In the following the Chebyshev collocation method is briefly described for the purpose of introducing notation. For an overview on spectral methods we refer to [17] and references contained therein.

The collocation method is based on polynomial interpolation of a function $u(x)$, and can be expressed as

$$u_N(x) = \sum_{j=0}^{N} u(x_j) l_j(x), \quad l_j(x) = \prod_{k=0, k\neq j}^{N} \frac{x - x_k}{x_j - x_k}, \quad j = 0, \ldots, N, \tag{1}$$

where x_j, $j = 0, \ldots, N$ are the collocation points and $l_j(x)$ are the Lagrange interpolation polynomials of degree N. To determine the derivative of the function $u(x)$ at the collocation points x_i, $u'(x_i)$, one can simply take the derivative of the Lagrange interpolating polynomial as

$$\frac{\partial u(x_i)}{\partial x} \approx \sum_{j=0}^{N} u(x_j) l_j'(x_i), \tag{2}$$

or, written compactly in the matrix-vector multiplication form as

$$\overrightarrow{u}' = \mathbf{D}\overrightarrow{u}, \tag{3}$$

where the differentiation matrix $D_{i,j} = l_j'(x_i)$. In the case of the Chebyshev collocation method based on the Gauss–Lobatto quadrature nodes, the collocation points are

$$x_i = -\cos(i\pi/N), \quad i = 0, \ldots, N. \tag{4}$$

To integrate the resulting system of ordinary differential equations (ODE) in time, we employ the third order Total Variation Diminishing (TVD) Runge–Kutta scheme [18]

$$\begin{aligned} u^{(1)} &= u^n + \Delta t L(u^n) \\ u^{(2)} &= \frac{3}{4}u^n + \frac{1}{4}u^{(1)} + \frac{1}{4}\Delta t L(u^{(1)}) \\ u^{n+1} &= \frac{1}{3}u^n + \frac{2}{3}u^{(2)} + \frac{2}{3}\Delta t L(u^{(2)}), \end{aligned} \tag{5}$$

in which L denotes the discretization of the spatial derivatives.

2.2 Dirac-Delta Approximation

In [14], a regularization technique based on a class of high-order, compactly supported piecewise polynomials is developed that regularizes the time-dependent, singular Dirac-Delta sources in spectral approximations of hyperbolic conservation laws. This regularization technique provides higher-order accuracy away from the singularity.

For the purpose of clarity in the following discussion, we shall define the compact support domain as $\Omega^{\varepsilon} = [-\varepsilon + x, x + \varepsilon]$ and $\Omega_i^{\varepsilon} = [-\varepsilon + x_i, x_i + \varepsilon]$ centered at $x = x_i$, and the Dirac-Delta polynomial kernel denoted by $\delta_{\varepsilon}^{m,k}(x)$ as the approximation of the Dirac-Delta function $\delta(x)$,

$$\delta_{\varepsilon}^{m,k}(x) = \begin{cases} \frac{1}{\varepsilon} P^{m,k}\left(\frac{x}{\varepsilon}\right) & x \in \Omega^{\varepsilon}, \\ 0 & \text{else}, \end{cases} \tag{6}$$

where $\varepsilon > 0$ is the support width or the scaling parameter. The function is generated by a multiplication of two lower degree polynomials that control the number of vanishing moments m, and the number of continuous derivatives at the endpoints of the compact support k, respectively. The $M = m + 2(k + 1)$ degree polynomial $P^{m,k}(x)$ is uniquely determined by the following conditions

$$\left(P^{m,k}\right)^{(i)}(\pm 1) = 0, \quad i = 1, ..., k, \tag{7}$$

$$\int_{-1}^{1} P^{m,k}(\xi) d\xi = 1, \tag{8}$$

$$\int_{-1}^{1} \xi^i P^{m,k}(\xi) d\xi = 0, \quad i = 1, ..., m, \tag{9}$$

in which (7) determines the number of continuous derivatives at the endpoints (k), (8) states that the function integrates to unity as a Dirac-Delta function, and (9) determines the number of vanishing moments (m). In Fig. 1, we show the polynomial approximation of the Dirac-Delta kernel $\delta_{\varepsilon}^{m,k}(x)$ with $(m, k) = (3, 8)$ and $(m, k) = (5, 8)$ with scaling parameter $\varepsilon = 1$. It has been shown that the Dirac-Delta approximation $\delta_{\varepsilon}^{m,k}(x)$ has an accuracy of $O(\varepsilon^{m+1})$.

The procedure for the generation of the polynomials $P^{m,k}(\xi)$ is described in [15]. A few examples for m=1 and m=3 vanishing moments and $k = 2$ continuous derivatives are given below.

– The polynomials with one vanishing moment $m = 1$ and with $k = 2$ continuous derivatives are

$$P^{1,0} = \frac{3}{4}(1 - \xi^2), \quad P^{1,1} = \frac{15}{16}(1 - 2\xi^2 + \xi^4), \quad P^{1,2} = \frac{35}{32}(1 - 3\xi^2 + 3\xi^4 - \xi^6). \tag{10}$$

– The polynomials with three vanishing moments $m = 3$ and with $k = 2$ continuous derivatives are

$$P^{3,0} = \frac{15}{32}(3 - 10\xi^2 + 7\xi^4), \quad P^{3,1} = \frac{105}{64}(1 - 5\xi^2 + 7\xi^4 - 3\xi^6), \tag{11}$$

$$P^{3,2} = \frac{315}{512}(3 - 20\xi^2 + 42\xi^4 - 36\xi^6 + 11\xi^8). \tag{12}$$

2.3 SIAC Filtering

The Smoothness-Increasing Accuracy-Conserving (SIAC) filter was developed in the context of superconvergence extraction and error reduction. SIAC filtering [19–22] exploits the idea of superconvergence in the underlying method to reduce oscillations in the errors, reduce errors and increase convergence rates. SIAC has its basis in the work by Bramble et al. [11] and Cockburn et al. [12]. It has been extended to include boundary filtering and nonuniform meshes [23–25] as well as to increase computational efficiency [26,27]. It has proven effective for applications in visualization [28,29].

The traditional application of SIAC filtering takes the numerical approximation, $u_h(x)$, and convolves it against a specially designed kernel,

$$u_h^\star(x) = \frac{1}{H}\int_{-\infty}^{\infty} K^{m+1,\ell}\left(\frac{y-x}{H}\right) u_h(y)\,dy, \tag{13}$$

where $K^{m+1,\ell}$ is a linear combination of m B-splines of order ℓ and H is a scaling typically related to a mesh quantity.

The symmetric form of the post-processing kernel can be written as

$$K^{m+1,\ell}(x) = \sum_{\gamma} c_\gamma^{m+1,\ell}\psi^{(\ell)}(x-\gamma), \tag{14}$$

where $\psi^{(\ell)}(x)$ is obtained by convolving the characteristic function over the interval $(-\frac{1}{2},\frac{1}{2})$ with itself $\ell+1$ times and the coefficients $c_\gamma^{m+1,\ell} \in \mathbb{R}$.

The form of the SIAC kernel is similar to the form of the Dirac-Delta kernel [14,15]. Primary properties of the SIAC that make the SIAC kernel suitable for regularization include:

- $\psi^{(\ell)}(x)$ can be expressed as a linear combination of Delta-functions, using the property $\frac{d^\alpha \psi^{(\ell)}(x)}{dx^\alpha} = \partial_H^\alpha \psi^{(\ell-\alpha)}(x)$, where ∂_H represents a divided difference.
- The SIAC kernel can reproduce polynomials of degree m. This is equivalent to the conditions
  - $\int_{\mathbb{R}} K^{m+1,\ell}(\xi)\,d\xi = 1$.
  - $\int_{\mathbb{R}} \xi^i K^{m+1,\ell}(\xi)\,d\xi = 0$ for $i = 1,\ldots,m$.

  These are similar to the conditions on the Dirac-Delta polynomial kernel. However, unlike this kernel, the SIAC kernel does not require the smoothness of the kernel even though it vanishes, at the endpoints of the compact support.

2.4 Dirac-Delta Filtering

In [16], an extension from [14], *singular source terms* are expressed as weighted summations of Dirac-Delta kernels that are regularized through approximation theory with convolution operators. The regularization is obtained by convolution with the high-order compactly supported Dirac-Delta kernel, (6), whose overall accuracy is controlled by the number of vanishing moments m, degree of smoothness k and length of the support ε. In this work, the Dirac-Delta kernel is used to regularize time dependent *discontinuous solutions*. Suppose the solution is given by the variable $u(x)$, $x \in [-1, 1]$. Then the filtered data, $\tilde{u}(x)$, follows from the convolution of $u(x)$ with the Dirac-Delta kernel as

$$\tilde{u}(x) = \int_{-1}^{1} u(\tau)\,\delta_\varepsilon^{m,k}(x-\tau)d\tau. \tag{15}$$

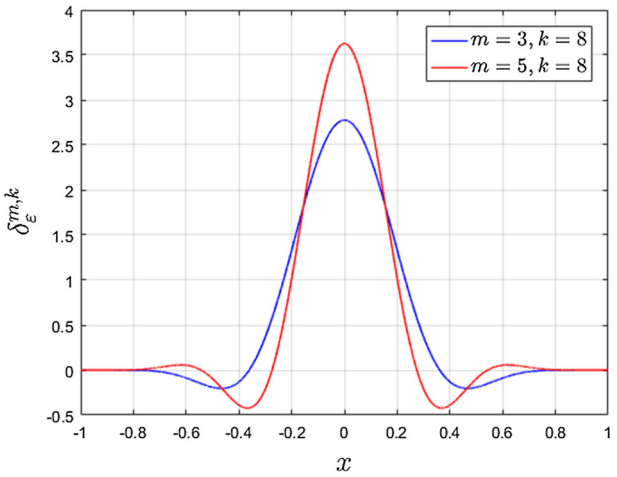

Fig. 1 Dirac-Delta kernel $\delta_\varepsilon^{m,k}$ for $(m, k) = (3, 8)$ and $(m, k) = (5, 8)$ with scaling parameter $\varepsilon = 1$

or, simply,

$$\tilde{u}(x) = \int_{\Omega^\varepsilon} u(\tau)\, \delta_\varepsilon^{m,k}(x - \tau) d\tau, \tag{16}$$

since the Dirac-Delta kernel is zero outside its compact support Ω^ε.

To apply the filtering operation, we need to choose the number of vanishing moments m, the number of continuous derivatives k and the scaling parameter ε.

We make the following notes:

- The number of vanishing moments, m, and support width, ε determine the accuracy of the Delta-kernel and by extension the error introduced by the filtering operation in smooth regions of the solution. In [16] it was proven that the filtering error is $O(\varepsilon^{m+1})$, provided the scaling parameter is $\varepsilon = O(N^{(-k/m+k+2)})$. The requirement on the scaling parameter follows from the fact that the error in the quadrature rule used to evaluate the convolution integral has to be smaller than the $O(\varepsilon^{m+1})$ accuracy of the Dirac-Delta approximation. More vanishing moments reduces the filtering error, however it requires a wider support, leading to a wider regularization zone.
- The smoothness of the Dirac-Delta kernel is controlled by the number of continuous derivatives at the endpoints, k. In [16] and [14] it is shown that k controls the smoothness of the transition between the regularized source and the solution and thus controls the order of convergence away from the source. When filtering the entire solution there is no such transition and thus the influence of k is minor. This is confirmed by numerical experiments.

Extension to two dimensions follows straightforwardly from the tensor product of the one-dimensional Delta-function:

$$\delta_\varepsilon^{m,k}(x, y) = \delta_\varepsilon^{m,k}(x) \otimes \delta_\varepsilon^{m,k}(y). \tag{17}$$

Figure 2 shows the two-dimensional equivalents of the one-dimensional kernels shown in Fig. 1. As in the one-dimensional case, the filtering is based on the convolution of the solution with the Delta-kernel,

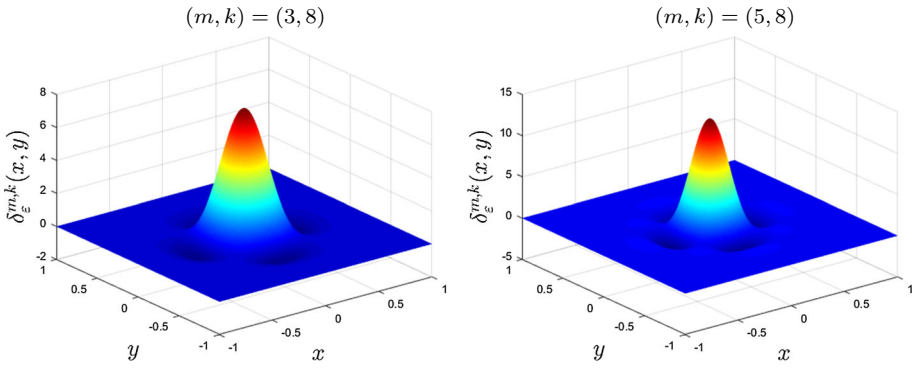

Fig. 2 Tensor product of the one-dimensional Dirac-Delta function, for (Left) $(m, k) = (3, 8)$ and (Right) $(m, k) = (5, 8)$ with scaling parameter $\varepsilon = 1$ (Color figure online)

$$\tilde{u}(x, y) = \int_{\Omega_x^\varepsilon} \int_{\Omega_y^\varepsilon} u(\tau, \eta) \delta_\varepsilon^{m,k}(x - \tau, y - \eta) d\tau d\eta. \tag{18}$$

2.5 Implementation of the Filtering Operation

Filtering of the interpolant of the solution (1), leads to,

$$\tilde{u}_N(x) = \int_{\Omega^\varepsilon} \left[\sum_{i=0}^{N} u(x_i) l_i(\tau) \right] \delta_\varepsilon^{m,k}(x - \tau) d\tau = \sum_{i=0}^{N} u(x_i) S_i(x), \tag{19}$$

after interchanging the summation and integration, where the filtering function $S_i(x)$ is

$$S_i(x) = \int_{\Omega^\varepsilon} l_i(\tau) \delta_\varepsilon^{m,k}(x - \tau) d\tau. \tag{20}$$

Hence, one has, at the collocation points,

$$\vec{\tilde{u}} = \mathbf{S} \vec{u}, \tag{21}$$

where the $(N + 1) \times (N + 1)$ filtering matrix $\mathbf{S}$ has elements

$$S_{i,j} = \int_{\Omega_j^\varepsilon} l_i(\tau) \delta_\varepsilon^{m,k}(x_j - \tau) d\tau. \tag{22}$$

In two dimensions, the filtering operation can be written compactly as

$$\tilde{\mathbf{U}} = \mathbf{S}_x \mathbf{U} \mathbf{S}_y^{\mathrm{T}}, \tag{23}$$

where $\mathbf{S}_x$ and $\mathbf{S}_y$ are the one-dimensional filtering matrix in $x-$ and $y-$ direction respectively and the superscript τ denotes transpose.

Remark 1 Near the boundaries, the compact support of the high-order Dirac-Delta function, $\delta_\varepsilon^{m,k}$, extends out of the domain and hence, the data can not be filtered in that case. This means that $\tilde{u}(x) = u(x)$ for $|x| > 1 - \varepsilon$. The filtering matrix S can be precomputed and stored for later use as long as the filter parameters remain unchanged.

2.6 Clenshaw–Curtis Quadrature

The one remaining important issue that needs to be addressed is how to evaluate the integrals in Eq. 19. Since the high-order Dirac-Delta function is a polynomial of degree $M = m+2(k+1)$ and the Lagrange interpolation polynomial is of degree $N-1$, the integrand is a polynomial of degree $M+N-1$ and can be evaluated analytically. Since this can become time-consuming for large N an appropriate quadrature rule is preferred. For this purpose Clenshaw–Curtis quadrature will be used, that is,

$$\int_{\Omega_i^\varepsilon} l_n(\tau)\delta_\varepsilon^{m,k}(x_i-\tau)d\tau \approx \sum_{q=0}^{Q} w_q l_n(x_q)\delta_\varepsilon^{m,k}(x_i-x_q). \tag{24}$$

where Q is the number of Chebyshev Gauss–Lobatto quadrature nodes used in the compact support domain Ω_i^ε, that is,

$$x_q = x_i - \varepsilon\cos\left(\frac{\pi q}{Q}\right), \quad q = 0,\ldots,Q, \tag{25}$$

and w_q are the corresponding weights. Clenshaw Curtis quadrature exactly evaluates polynomials of degree $Q-1$. Hence, if one takes $Q = M+N$, the integrals are evaluated exactly. Also, the weights w_q can be precomputed using fast Fourier transform (FFT).

2.7 Shock Capturing with Dirac-Delta Filtering

The theoretical requirement for the scaling parameter, $\varepsilon = \mathcal{O}(N^{(-k/m+k+2)})$, to assure $\mathcal{O}(\varepsilon^{m+1})$ accuracy in the convolution operation is based on the requirement that the error in the quadrature rule has to be smaller than the error in the Dirac-Delta approximation [16]. Since the convolution integrals in this work are solved exactly using Clenshaw–Curtis quadrature, this criterium can be relaxed. For shock capturing we choose the scaling parameter to be proportional to the grid spacing and to guarantee that at least two neighboring collocation points are located inside the compact support. In this case, the scaling parameter will be expressed in terms of the number of points N_d the kernel spans at the center of the domain $x = x_{N/2}$, assuming N is even, that is,

$$\varepsilon = \sin\left(\pi N_d/(2N)\right). \tag{26}$$

The value of N_d is determined empirically and chosen to ensure stable converging results. It depends on the number of vanishing moments m of the Dirac-Delta kernel and whether the filter is applied in a linear or non-linear equation. For implementation in the linear advection equation, only the initial condition is filtered while for nonlinear PDE's, such as the Burgers' equation and the Euler equations, the solution is filtered at the end of every Runge–Kutta time step. This is because of the formation of a finite space-time singularity by the nonlinearity of the equations. Filtering can lead to smearing of the discontinuity and the summation of filter errors in smooth regions. On the other hand, if the N_d is chosen to be too small, the filter will not be able to suppress the Gibbs oscillations effectively which leads to a nonlinear growth of the high modes. Since the scheme has no other dissipation mechanism, it will become unstable in time. We find that if we filter at every Runge–Kutta time step, N_d (as reflected in the size of ϵ) can be chosen to be quite small (about 2–6) to ensure the sharpness of the shock transition while maintaining stability and preserving high-order resolution away from a discontinuity

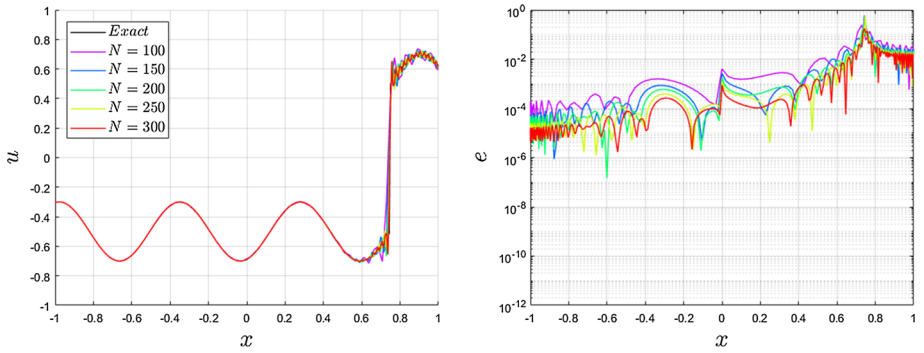

Fig. 3 Linear advection equation: analytical and spectral solution (Left), and pointwise error (Right) at time $t = 1$, for the five different grids without filter

Remark 2 Near the boundary the filter cannot be convoluted due to the symmetry of the convolution kernel. In this paper those few points are reset to be the exact solution for the nonlinear PDEs in order to isolate and study solely the effects of the Dirac-Delta kernels. Furthermore, to avoid the effect of variable time step Δt, we fixed the stable time step of $\Delta t = 1 \times 10^{-5}$ in all the simulations performed below in order to be able to compare results.

3 Numerical Tests

In this section, we conduct a range of test cases for the linear advection equations, the Burger's equations and the Euler equation in one- and two-dimensions. The filter we use is based on the Dirac-Delta kernel with $m = 3$ zero moment, $k = 8$ smoothness and $N_d = 13$, unless otherwise noted.

3.1 Advection Equation

3.1.1 1D Advection Equation

We start by considering the one-dimensional linear advection equation with a discontinuous initial condition on the domain $-1 < x < 1$ as follows,

$$\begin{aligned} &\frac{\partial u}{\partial t} + \frac{\partial u}{\partial x} = 0, \\ &u(x,0) = \begin{cases} 0.2\sin(10x) - 0.5 & x \le -0.25 \\ 0.2\sin(10x) + 0.5 & x > -0.25 \end{cases}, \\ &u(-1,t) = 0.2\sin(10(-1-t)) - 0.5. \end{aligned} \tag{27}$$

Without filtering, Gibb's oscillations pollute the solutions as can be seen in Fig. 3. In the vicinity of the discontinuity, the error for all N have a similar magnitude. Away from the discontinuity a grid refinement leads to a reduction of the error.

Next, we filter the initial condition and then advect the solution without further filtering. Since the advection equation is linear, this initial filtered solution and associated error is simply advected as shown in Fig. 4. Since the solution is advected for a unit time, the point-

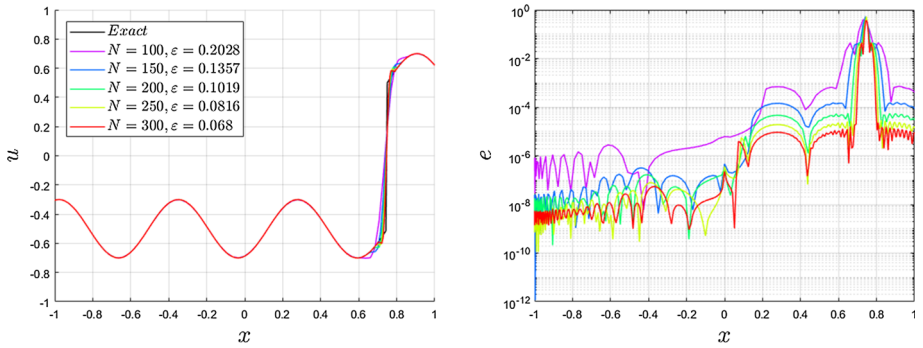

Fig. 4 Linear advection equation: analytical and spectral solution (Left), and pointwise error (Right) at time $t = 1$, for the five different grids with $(m, k) = (3, 8)$ and $N_d = 13$

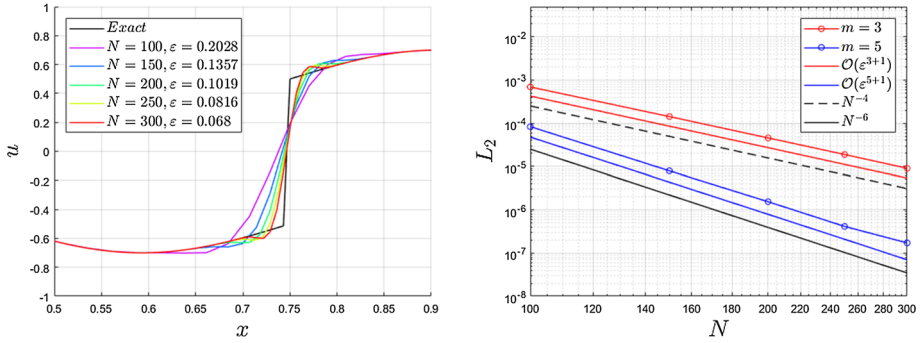

Fig. 5 Linear advection equation: detail view of regularization zone (Left) and error convergence at $x = 0.28$ compared to the theoretical value $O(\varepsilon^{m+1})$ (Right) for the five different grids with $(m, k) = (3, 8)$, $N_d = 13$. The case $(m, k) = (5, 8)$, $N_d = 17$ is included to show the effect of m

wise error for $x > 0$ identifies the filter error, while for $x < 0$, the solution behaves according to the spectral solution.

The filter solution captures the discontinuity, while significantly improving upon the error behavior away from the discontinuity (compare Figs. 3 and 4). In fact, outside the regularization zone the error convergence follows the theoretical estimate of $O(\varepsilon^{m+1})$. Figure 5, confirms this finding by plotting the error versus N at $x = 0.28$ for $m = 3$ and $m = 5$. The filter error can hence be decreased by according to a increase of m. We note that this does come at the expense of a wider regularization zone (Fig. 5).

3.1.2 2D Advection Equation

In two dimensions, we test the filter for the linear advection equation on the $-1 \leq x, y \leq 1$ square domain,

$$\frac{\partial u}{\partial t} + \frac{\partial u}{\partial x} + \frac{\partial u}{\partial y} = 0, \tag{28}$$

$$u(x, y, 0) = \begin{cases} \cos(4\pi\sqrt{x^2 + (y + 0.5)^2}^2)), & \text{if } x^2 + (y + 0.5)^2 < 0.25^2 \\ 0 \quad \text{otherwise,} \end{cases} \tag{29}$$

Like for the 1D test case, the discontinuous initial condition is first filtered according to (23) The filtered initial condition is consequently advected (Fig. 6). The local error in Fig. 7

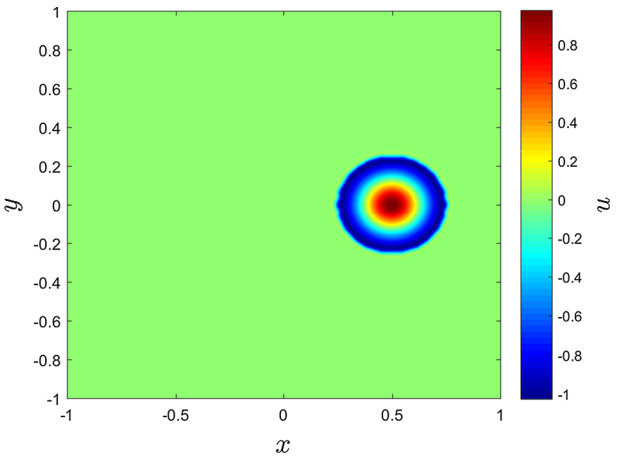

Fig. 6 2D Advection equation: contour plot of u at $t = 0.5$ for $(m, k) = (3, 8)$ and $N_d = 13$

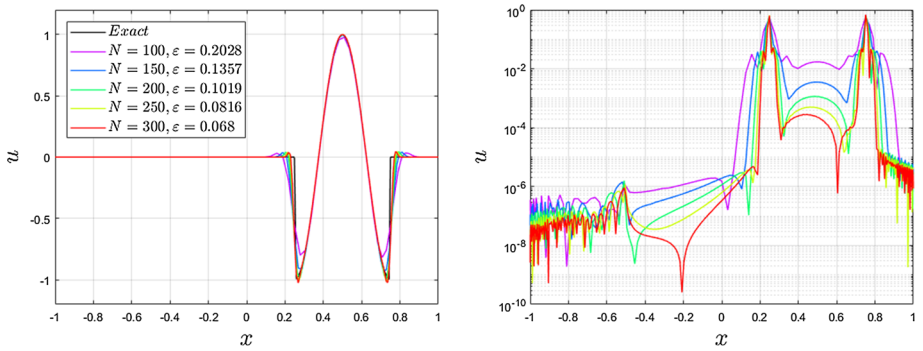

Fig. 7 2D Advection equation: numerical solution (Left) and error (Right) along $y = 0$ at $t = 0.5$, for the five different grids for $(m, k) = (3, 8)$ and $N_d = 13$

shows that in 2D the discontinuity is captured accurately and the filtered solution converges according to theory. This is analogue to the 1D case.

In order to check the supposed radial symmetry of the solution around $x, y = (0.5, 0)$, a scatterplot of the solution and the error versus the radial coordinate centered at the circular symmetric initial condition is shown in Fig. 8. Because the tensor product of the Dirac-Delta kernel is not radially symmetric, it is likely causing some of radial error variation. The error, however, reduces rapidly away from the regularization zone, and hence has high-order resolution.

3.1.3 2D Rotating Problem

To further investigate the effect of tensorial Dirac-Delta on radial symmetry, we consider the rotating problem,

$$\frac{\partial u}{\partial t} - y\frac{\partial u}{\partial x} + x\frac{\partial u}{\partial y} = 0, \tag{30}$$

with the same initial condition and filter as in (29).

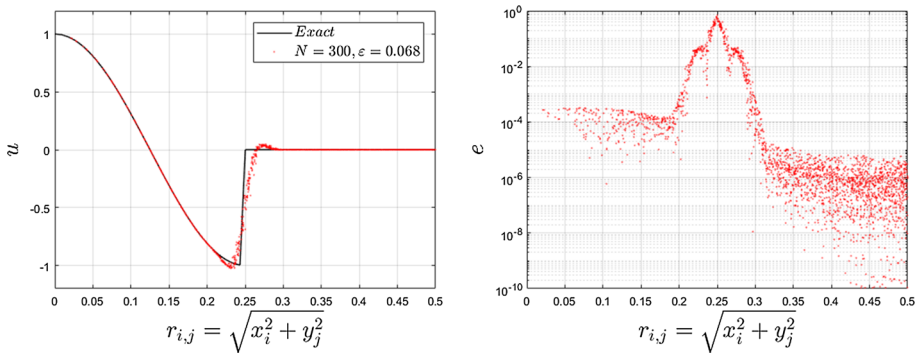

Fig. 8 2D Advection equation: scatter plot of numerical solution (Left) and error (Right) at $t = 0.5$, for $N = 300$ for $(m, k) = (3, 8)$ and $N_d = 13$

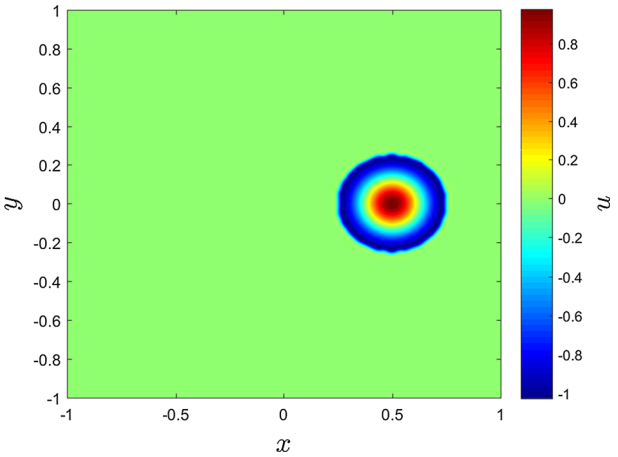

Fig. 9 2D Rotating problem: contour plot of u at $t = \pi/2$ for $(m, k) = (3, 8)$ and $N_d = 13$

Inspecting the solution in Figs. 9 and 10, shows that the discontinuities are captured with the same level of smoothness and error convergence trends are the same. A scatterplot of the solution and error in Fig. 11 shows some error variation, but with clear trends and higher-order resolution.

3.2 Burger's Equation

To test a non-linear case, we consider the Burgers' equation,

$$\frac{\partial u}{\partial t} + \frac{1}{2}\frac{\partial u^2}{\partial x} = 0, \quad u(x, 0) = -\sin(\pi x), \quad u(\pm 1, t) = 0 \tag{31}$$

Because the equation is non-linear, and a discontinuity inherent to the solution forms in time, we now have to filter the solution at the end of every Runge–Kutta time step. In the results below we use $N_d = 2.5$.

Figure 12 shows that the Dirac-delta filtering effectively captures the shock and gives a stable solution. A clearly visible overshoot is however introduced. Increasing the number of vanishing moments reduces the overshoot (not shown here).

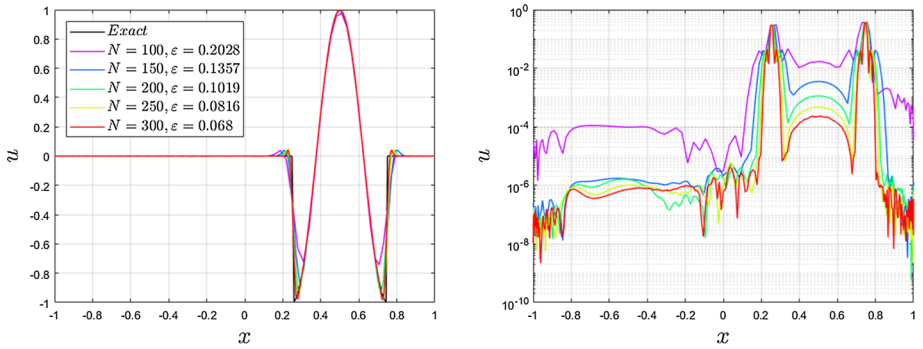

Fig. 10 2D Rotating problem: numerical solution (Left) and error (Right) along $y = 0$ at $t = \pi/2$, for the five different grids for $(m, k) = (3, 8)$ and $N_d = 13$

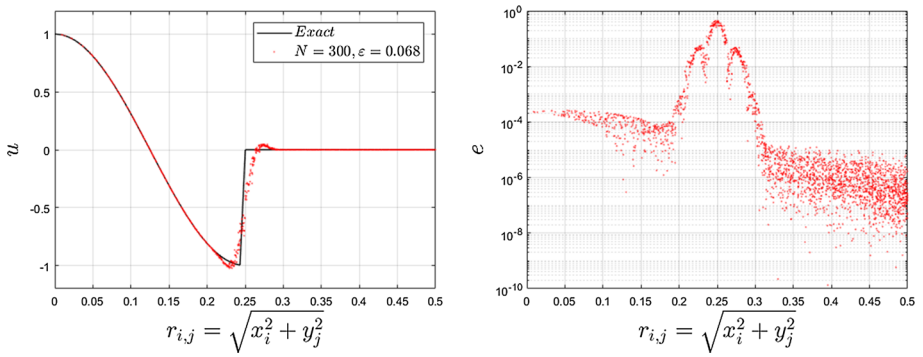

Fig. 11 2D Rotating problem: scatter plot of numerical solution (Left) and error (Right) at $t = \pi/2$, for $N = 300$ for $(m, k) = (3, 8)$ and $N_d = 13$

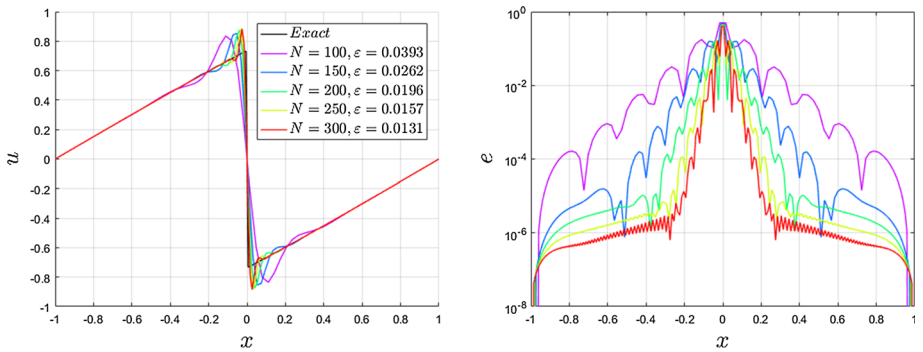

Fig. 12 Burger's equation: numerical solution (Left), and pointwise error (Right) at time $t = 1$, for the five different grids with $(m, k) = (3, 8)$ and $N_d = 2.5$

The error (Fig. 12) that is introduced by regularization at the shock location is smeared over the domain by the multiple application of the filter at each time step. For the values of N_d used here, the smearing is small. The smearing effect increases with increasing support

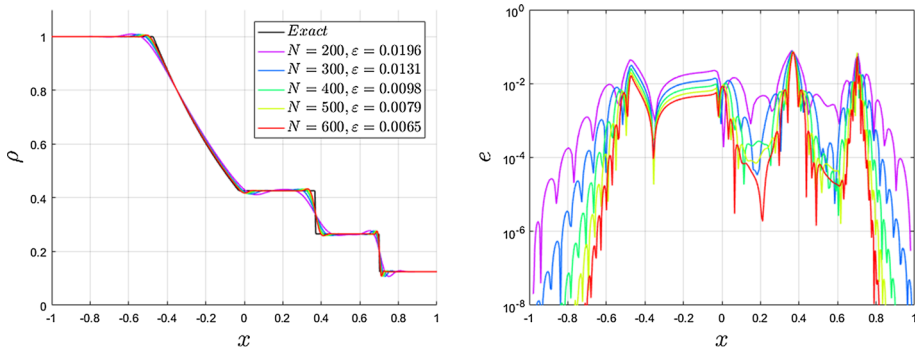

Fig. 13 Sod's shock tube problem: analytical solution, spectral solution (Left) and pointwise error (Right) of the density at $t = 0.4$, for the five different grids for $(m, k) = (3, 8)$ and $N_d = 2.5$

width. We note that extending the simulation time until $t = 5$ does not change the error much as compared to error at $t = 1$. Only the shock is slightly more dissipated.

3.3 Euler Equations

To test the filter on systems of non-linear PDEs, we consider the Euler equations governing inviscid flow. In two dimensions and in a strong conservation form they are given as:

$$\mathbf{Q}_t + \mathbf{F}_x + \mathbf{G}_y = 0, \tag{32}$$

with

$$\begin{aligned} &\mathbf{Q} = (\rho, \rho u, \rho v, E)^T,\ \mathbf{F} = (\rho u, \rho u^2 + P, \rho uv, (E + P)u)^T, \\ &\mathbf{G} = (\rho u, \rho uv, \rho v^2 + P, (E + P)v)^T, \end{aligned} \tag{33}$$

where $\mathbf{Q}$ are the conservative variables, $\mathbf{F}$ and $\mathbf{G}$ are the fluxes in the x- and y-directions, and the equation of state is $P = (\gamma - 1)\left(E - \frac{1}{2}\rho(u^2 + v^2)\right)$ with $\gamma = 1.4$. The ρ, u, v, P, and E are the density, velocities in x- and y-directions, pressure, and total energy respectively. We test the filter for both one-dimensional and two-dimensional solutions of these equations.

3.3.1 Sod's Shock Tube Problem

In Fig. 13, we show the density of the classical Sod shock tube problem. Here, the conservative variables are filtered by the Dirac-Delta filter with $N_d = 2.5$ at every Runge–Kutta time step with several number of collocation grid points. The solutions show that both the shock and the contact are effectively captured and the error decays rapidly from the discontinuities (shock, contact discontinuity, and rarefactions) sufficiently far away from the discontinuity.

3.3.2 Shu–Osher Problem

Shu–Osher's Problem has initial conditions $(\rho_L, P_L, u_L) = (27/7, 31/3, 4\sqrt{35/9})$ and $(\rho_R, P_R, u_R) = (1 + 0.2\sin(25x), 1, 0)$. Again, the conserved quantities are filtered every time-step using the filtering matrix. For the results below we use $m = 5$, $N_d = 6.5$ in order to limit the error introduced in the entropy-wave. A 5th order WENO-solution on 10,000 points is used to serve as a reference 'exact' solution (Figs. 14, 15).

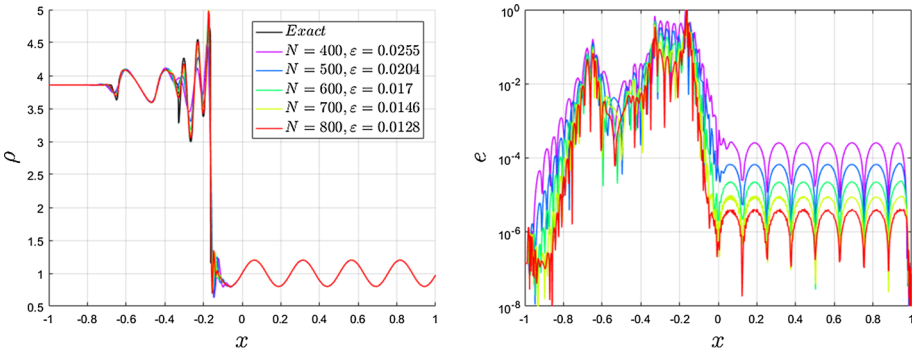

Fig. 14 Shu–Osher problem: analytical solution, spectral solution (Left) and pointwise error (Right) of the density at $t = 0.18$, for the five different grids for $(m, k) = (5, 8)$ and $N_d = 6.5$

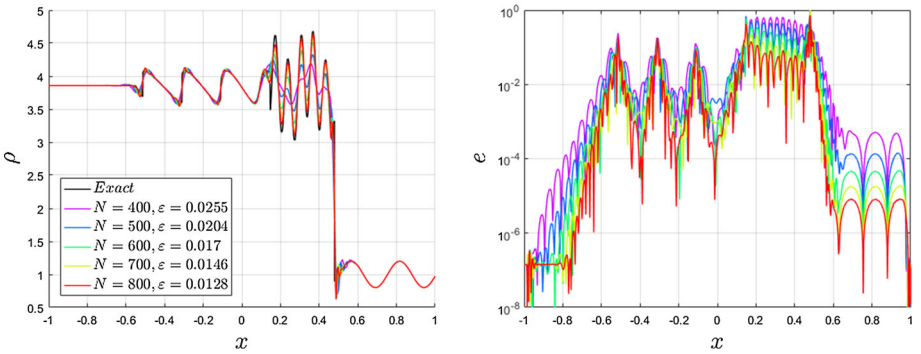

Fig. 15 Shu–Osher problem: analytical solution, spectral solution (Left) and pointwise error (Right) of the density at $t = 0.36$, for the five different grids for $(m, k) = (5, 8)$ and $N_d = 6.5$

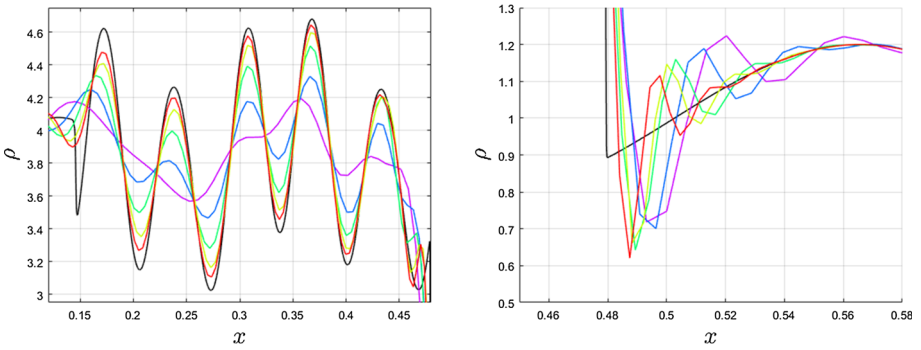

Fig. 16 Shu–Osher problem: detail view of the entropy wave (Left) and the regularization zone (Right) at $t = 0.36$, for the five different grids for $(m, k) = (5, 8)$ and $N_d = 6.5$

The solution shows that the filter effectively captures the shock while the kernel with $m = 5$ vanishing moments ensures high resolution behind the shock. Figure 16 provides a detail view of the entropy wave (Left) and the regularization zone (Right).

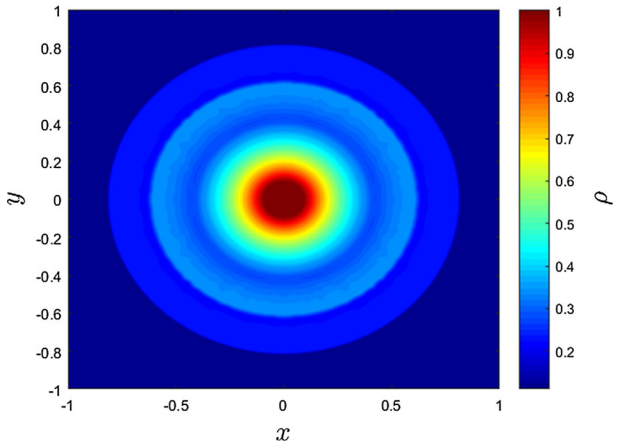

Fig. 17 Explosion problem: contour plot of the density at $t = 0.25$ for $(m, k) = (3, 8)$ and $N_d = 2.5$

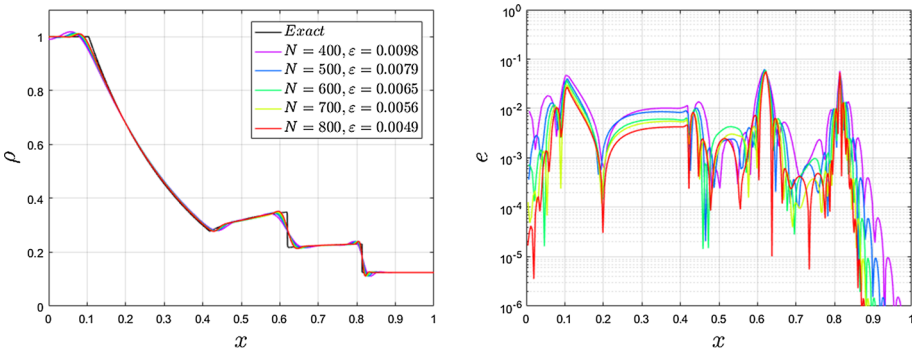

Fig. 18 Explosion problem: numerical solution (Left) and error (Right) along the radial line at $t = 0.25$, for the five different grids for $(m, k) = (3, 8)$ and $N_d = 2.5$

3.4 Explosion Problem

As a 2D test case, the explosion problem is considered. This problem is governed by the 2D Euler equations, (32). The equations are solved on a 2.0×2.0 square domain in the $x - y$ plane. The initial condition consists of the region inside of a circle with radius $R = 0.4$ centered at $(0, 0)$ and the region outside of the circle. The flow variables are constant in each of these regions and are separated by a circular discontinuity at time $t = 0$. The two constant states are chosen as:

$$\rho_{in} = 1.0 \quad \rho_{out} = 0.125, \tag{34}$$

$$p_{in} = 1.0 \quad p_{out} = 0.1, \tag{35}$$

$$u_{in} = 0.0 \quad u_{out} = 0.0, \tag{36}$$

$$v_{in} = 0.0 \quad v_{out} = 0.0, \tag{37}$$

where the subscripts in and out denote values inside and outside the circle, respectively. The approach described by Eleuterio [30] is used to serve as an exact solution. For the results we used a kernel with $(m, k) = (3, 8)$ and $N_d = 2.5$ (Figs. 17, 18).

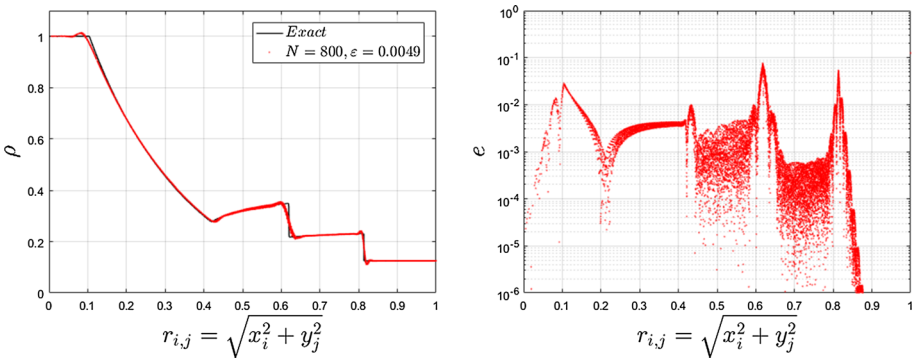

Fig. 19 Explosion problem: scatter plot of numerical solution (Left) and error (Right) at $t = 0.25$, for $N = 800$ for $(m, k) = (3, 8)$ and $N_d = 2.5$

The contour plot of the density shows that the symmetry of the flow is captured on the 2D Cartesian grid. Since the solution to the 2D explosion problem is radially symetric and the 2D Dirac-Delta kernel is asymmetrical, Fig. 2, it is interesting to see how well the radial symmetry is captured. In order to do so a scatter plot of the solution and error is made. A sample of the solution $\rho_{i,j} = \rho(x_i, y_j)$ is plotted versus the radial coordinate. An error plot is included as well. The error follows a clear trend with the most variation in between the discontinuities (Fig. 19).

4 Conclusions and Future Work

In this paper, the use of high-order Dirac-Delta function based filter for the regularization of shocks and discontinuities in combination with a global spectral method is investigated. We have shown that these filters are able to effectively capture shocks while maintaining high resolution in smooth areas of the solution. Through a tensorial implementation the filter extends easily from one-dimension to two-dimensions. Radial asymmetry of the tensorial implementation is a possible cause for some error variation but it does not affect higher-order resolution.

We are extending the filter operation for use in discontinuous spectral element methods and expect to report on this soon.

References

1. Shu, C.W., Osher, S.: Efficient implementation of essentially non-oscillatory shock-capturing schemes. J. Comput. Phys. **77**, 439–471 (1988)
2. Cockburn, B.: Devising discontinuous galerkin methods for non-linear hyperbolic conservation laws. J. Comput. Appl. Math. **128**, 187–204 (2001)
3. Cockburn, B., Shu, C.W.: Runge–Kutta discontinuous galerkin methods for convection-dominated problems. J. Sci. Comput. **16**, 173–261 (2001)
4. Dumbser, M., Zanotti, O., Loubére, R., Diot, S.: A posteriori subcell limiting of the discontinuous Galerkin finite element method for hyperbolic conservation laws. J. Comput. Phys. **278**, 47–75 (2014)
5. Chaudhuri, A., Jacobs, G.B., Don, W.S., Abassi, H., Mashayek, F.: Explicit discontinuous spectral element method with entropy generation based artificial viscosity for shocked viscous flows. J. Comput. Phys. **332**, 99–117 (2017)

6. Hughes, T.J., Franca, L., Mallet, M.: A new finite element formulation for computational fluid dynamics: I. Symmetric forms of the compressible euler and Navier–Stokes equations and the second law of thermodynamics. Comput. Methods Appl. Mech. Eng. **54**, 223–234 (1986)
7. Guermond, J.L., Pasquetti, R., Popov, B.: Entropy viscosity method for nonlinear conservation laws. J. Comput. Phys. **230**, 4248–4267 (2011)
8. Persson, P.O., Peraire, J.: Sub-cell shock capturing for discontinuous Galerkin methods. Proceedings of the 44th AIAA Aerospace Sciences Meeting and Exhibit, January 2006. AIAA-2006-112 (2006)
9. Don, W.S.: Numerical Study of pseudospectral methods in shock wave applications. J. Comput. Phys. **110**, 103–111 (1994)
10. Vandeven, H.: Family of spectral filters for discontinuous problems. J. Sci. Comput. **6**(2), 159–192 (1991)
11. Bramble, J.H., Schatz, A.H.: Higher order local accuracy by averaging in the finite element method. Math. Comput. **31**, 94–111 (1977)
12. Cockburn, B., Luskin, M., Shu, C.W., Sli, E.: Enhanced accuracy by post-processing for finite element methods for hyperbolic equations. Math. Comput. **72**, 577–606 (2003)
13. Mock, M.S., Lax, P.D.: The computation of discontinuous solutions of linear hyperbolic equations. Commun. Pure Appl. Math. **18**, 423–430 (1978)
14. Suarez, J.P., Jacobs, G.B., Don, W.S.: A high-order Dirac-delta regularization with optimal scaling in the spectral solution of one-dimensional singular hyperbolic conservation laws. SIAM J. Sci. Comput. **36**, 1831–1849 (2014)
15. Tornberg, A.K.: Multi-dimensional quadrature of singular and discontinuous functions. BIT **42**, 644–669 (2002)
16. Suarez, J.P., Jacobs, G.B.: Regularization of singularities in the weighted summation of Dirac-delta functions for the spectral solution of hyperbolic conservation laws. J. Sci. Comput. arXiv:1611.05510
17. Gottlieb, S., Hesthaven, J., Gottlieb, D.: Spectral Methods for Time-Dependent Problems. Cambridge University Press, Cambridge (2007)
18. Gottlieb, S., Shu, C.W.: Total variation diminishing Runge-Kutta schemes. Math. Comput. **67**(221), 73–85 (1998)
19. Ryan, J.K., Shu, C.W., Atkins, H.L.: Extension of a post-processing technique for discontinuous Galerkin methods for hyperbolic equations with application to an aeroacoustic problem. SIAM J. Sci. Comput. **26**, 821–843 (2004)
20. King, J., Mirzaee, H., Ryan, J.K., Kirby, R.M.: Smoothness-increasing accuracy-conserving (SIAC) filtering for discontinuous Galerkin solutions: Improved errors versus higher-order accuracy. J. Sci. Comput. **53**, 129–149 (2012)
21. Curtis, S., Kirby, R.M., Ryan, J.K., Shu, C.W.: Post-processing for the discontinuous Galerkin method over non-uniform meshes. SIAM J. Sci. Comput. **30**, 272–289 (2007)
22. Ji, L., van Slingerland, P., Ryan, J.K., Vuik, C.: Superconvergent error estimates for a position-dependent smoothness-increasing accuracy-conserving filter for DG solutions. Math. Comput. **83**, 2239–2262 (2014)
23. Mirzaee, H., Ji, L., Ryan, J.K., Kirby, R.M.: Smoothness-increasing accuracy-conserving (SIAC) post-processing for discontinuous Galerkin solutions over structured triangular meshes. SIAM J. Numer. Anal. **49**, 1899–1920 (2011)
24. Ryan, J.K., Shu, C.W.: On a one-sided post-processing technique for the discontinuous Galerkin methods. Methods Appl. Anal. **10**, 295–307 (2003)
25. van Slingerland, P., Ryan, J.K., Vuik, C.: Position-dependent smoothness-increasing accuracy-conserving (SIAC) filtering for accuracy for improving discontinuous Galerkin solutions. SIAM J. Sci. Comput. **33**, 802–825 (2011)
26. Mirzaee, H., Ryan, J.K., Kirby, R.M.: Quantification of errors introduced in the numerical approximation and implementation of smoothness-increasing accuracy-conserving (SIAC) filtering of discontinuous Galerkin (DG) fields. J. Sci. Comput. **45**, 447–470 (2010)
27. Mirzaee, H., Ryan, J.K., Kirby, R.M.: Efficient implementation of smoothness-increasing accuracy-conserving (SIAC) filters for discontinuous Galerkin solutions. J. Sci. Comput. **52**, 85–112 (2012)
28. Steffan, M., Curtis, S., Kirby, R.M., Ryan, J.K.: Investigation of smoothness-increasing accuracy-conserving filters for improving streamline integration through discontinous fields. IEEE-TVCG **14**, 680–692 (2008)
29. Walfisch, D., Ryan, J.K., Kirby, R.M., Haimes, R.: One-sided smoothness-increasing accuracy-conserving filtering for enhanced streamline integration through discontinuous fields. J. Sci. Comput. **38**, 164–184 (2009)
30. Toro, E.F.: Riemann Solvers and Numerical Methods for Fluid Dynamics. Springer, Berlin (2009)